NASA TECHNICAL NOTE

NASA TN D-7605

NASA TN D-7605

NUMERICAL CALCULATIONS OF TWO-DIMENSIONAL, UNSTEADY TRANSONIC FLOWS WITH CIRCULATION

by Richard M. Beam and R. F. Warming

Ames Research Center
Moffett Field, Calif. 94035

NATIONAL AERONAUTICS AND SPACE ADMINISTRATION • WASHINGTON, D. C. • FEBRUARY 1974

1. Report No.	2. Government Accession No.	3. Recipient's Catalog No.
D- 7605		

4. Title and Subtitle	5. Report Date
NUMERICAL CALCULATIONS OF TWO-DIMENSIONAL, UNSTEADY TRANSONIC FLOWS WITH CIRCULATION	February 1974
	6. Performing Organization Code
7. Author(s)	8. Performing Organization Report No.
Richard M. Beam and R. F. Warming	A-5265
	10. Work Unit No.
9. Performing Organization Name and Address	501-06-02-01-00-21
Ames Research Center Moffett Field, Calif. 94035	11. Contract or Grant No.
	13. Type of Report and Period Covered
12. Sponsoring Agency Name and Address	Technical Note
National Aeronautics and Space Administration Washington, D. C., 20546	14. Sponsoring Agency Code

15. Supplementary Notes

16. Abstract

The feasibility of obtaining two-dimensional, unsteady transonic aerodynamic data by numerically integrating the Euler equations is investigated. An explicit, third-order-accurate, noncentered, finite-difference scheme is used to compute unsteady flows about airfoils. Solutions for lifting and nonlifting airfoils are presented and compared with subsonic linear theory. The applicability and efficiency of the numerical indicial function method are outlined. Numerically computed subsonic and transonic oscillatory aerodynamic coefficients are presented and compared with those obtained from subsonic linear theory and transonic wind-tunnel data. Proposed areas for future investigation are indicated.

17. Key Words (Suggested by Author(s))		18. Distribution Statement
Flutter	Oscillatory transonic flow	
Transonic flow	Unsteady aerodynamics	Unclassified — Unlimited
Transonic flutter	Upwind differencing	
Computational fluid dynamics		Cat.12

19. Security Classif. (of this report)	20. Security Classif. (of this page)	21. No. of Pages	22. Price*
Unclassified	Unclassified	27	$3.00

*For sale by the National Technical Information Service, Springfield, Virginia 22151

Page Intentionally Left Blank

SYMBOLS

AR	aspect ratio
c	chord length (also wave speed in the appendix)
Δc	deficiency function $\Delta c(\tau) = c(\infty) - c(\tau)$
$c^R(\tau), c^S(\tau)$	response functions for ramp and step, respectively
c_{ℓ_q}, c_{m_q}	indicial lift and moment coefficients due to pitching
$c_{\ell_\alpha}, c_{m_\alpha}$	indicial lift and moment coefficients due to angle-of-attack change without pitching
c_p	pressure coefficient, $\frac{p - p_\infty}{q_o}$
c_p^*	critical pressure coefficient
$c_{p_{\alpha_h}}$	absolute value of pressure coefficient for oscillating sinking airfoil
e	total energy per unit volume
E	shift operator
F, G, U	vectors defined in equations (3)
$g(k)$	amplification factor
k	reduced frequency, $k = \frac{\omega c}{2U_\infty}$ (also wave number in the appendix)
k_{max}, k_{min}	maximum and minimum numerical resolvable reduced frequencies
$L_1, L_2, \ldots, M_1, \ldots$	oscillatory aerodynamic coefficients defined in equations (8)
$m_\theta, m_{\dot\theta}$	dimensionless stiffness and damping coefficients for pitching motion; $m_\theta = k^2 M_3$, $m_{\dot\theta} = \frac{kM_4}{2}$
M	Mach number
p	pressure
Δp	differential pressure between upper and lower surfaces

q_o	free-stream dynamic pressure, $q_o = \frac{1}{2}\rho_\infty U_\infty^2$
$S(z)$	numerical stability polynomial
t	time
u,v	velocity components
U_∞	free-stream velocity
$v^n(k)$	Fourier component
x,y	Cartesian coordinates
α	angle of attack
γ	ratio of specific heats
Γ	circulation
δ,Δ,∇,μ	difference operators
Δ	grid spacing (also difference operator in the appendix)
ϵ	body thickness/chord ratio
ζ_h	phase angle for pressure coefficient of oscillating sinking airfoil
$\mu(p)$	spatial derivative coefficients, equation (A7)
θ	angle of pitch relative to horizontal
ν	Courant number
ρ	density
σ	eigenvalue of linearized gasdynamic equations
τ	dimensionless time, $\tau = \frac{u_\infty t}{c}$
τ_o	ramp function characteristic time
ω	frequency of oscillation (also general numerical free parameter in the appendix)
$\omega_x,\omega_{xs},\omega_y$	parameters of numerical method

Subscripts and Superscripts

n	time index
j,k	x,y spatial indices
q	pitching motion
α	sinking motion
∞	free-stream conditions

NUMERICAL CALCULATIONS OF TWO-DIMENSIONAL, UNSTEADY TRANSONIC FLOWS WITH CIRCULATION

Richard M. Beam and R. F. Warming

Ames Research Center

SUMMARY

The feasibility of obtaining two-dimensional, unsteady transonic aerodynamic data by numerically integrating the Euler equations is investigated. An explicit, third-order-accurate, noncentered, finite-difference scheme is used to compute unsteady flows about airfoils. Solutions for lifting and nonlifting airfoils are presented and compared with subsonic linear theory. The applicability and efficiency of the numerical indicial function method are outlined. Numerically computed subsonic and transonic oscillatory aerodynamic coefficients are presented and compared with those obtained from subsonic linear theory and transonic wind-tunnel data. Proposed areas for future investigation are indicated.

INTRODUCTION

The transonic flight regime is especially susceptible to dynamic and aeroelastic instabilities because of (1) the maxima of the lift-slope curves and (2) the large time lag between surface motions and aerodynamic forces that occur for bodies moving at near sonic speeds. These facts, coupled with the recent development of aircraft with transonic cruise speeds, have renewed interest in the solution of unsteady transonic aerodynamic problems.

Unsteady subsonic and supersonic aerodynamic coefficients generally have been satisfactorily determined from linear theory (refs. 1-5). The transonic aerodynamic coefficients for airfoils can be obtained from linear theory if (refs. 6-8)

$$\varepsilon \ll 1 , \quad k\varepsilon \ll 1 , \quad M_\infty \varepsilon \ll 1, \quad kM_\infty \varepsilon \ll 1$$

and if either

$$\begin{aligned} |M_\infty - 1| &\gg \varepsilon^{2/3} \\ k &\gg \varepsilon^{2/3} \end{aligned} \tag{1}$$

where k is the reduced frequency of oscillation; ε, the thickness ratio; and M_∞, the free-stream Mach number. This linearization is developed from the small perturbation of a steady-state flow that is *uniform*. If the airfoil is

not thin, the steady-state flow field will not be uniform but will depend on the nonlinear aerodynamic effects. There is still the possibility of a linearization of the small perturbation unsteady motion about the nonuniform steady state. The resulting equations, however, are still formidable since the nonlinear equations must be solved for the steady state and the partial differential equations with spatially variable coefficients for the unsteady perturbation. (This latter linearization is discussed in section IV.)

Analytical solutions for the nonlinear transonic *steady* flow equations are very limited and generally are restricted to approximate solutions to the small perturbation potential equation. The complexity of the unsteady nonlinear equations (low-frequency small perturbation or all frequency large perturbation) or the unsteady linear equations with variable coefficients (small perturbation about nonuniform flow field) further restricts the development of analytical solutions. The development of large computers and the refinement of numerical methods for solving difference equations have led to the solution of many heretofore unsolved aerodynamic problems. The numerical solution of steady-state transonic inviscid flows in both two and three space dimensions is well established (refs. 9-12). Similar numerical schemes seem the most promising for obtaining solutions to complex unsteady transonic flow problems.

Time accurate numerical differencing schemes are available (refs. 9 and 13) (although their primary application has been to solve steady-state equations[1]) and are probably the most efficient (least computer time) method for solving the unsteady nonlinear equations. While relaxation methods generally offer more efficient solution to steady-state transonic problems, they require one more dimension (artificial time) for time accuracy and would probably be less efficient than the time accurate methods.

The most efficient method for numerically solving the linear variable coefficient equations (small perturbation about nonuniform steady state) is not evident. For time histories of general body motion, the time accurate methods probably are more efficient (for the same reason as in the nonlinear case). If the desired result is the oscillatory aerodynamic coefficients, both time accurate solutions and relaxation methods have their advantages. The relaxation methods do not require more dimensions than the time accurate methods since real time can be eliminated (harmonic motion) while artificial time is retained. Each frequency requires a separate solution to the relaxation problem. On the other hand, one solution to the time accurate method with an indicial (step) input for the motion can be used to obtain coefficients for all frequencies by a Fourier transform of the indicial response (which requires very little computer time). The time accurate indicial function approach is used here (sections IV and V). The steady-state solution to the nonlinear equations, which provides variable coefficients for the linear problem, is obtained most efficiently by relaxation. However, the steady-state solution was

[1]The limit of the time accurate methods as time becomes very large is the steady-state solution (ref. 9). For supersonic flows, the steady-state solution is obtained more efficiently by taking advantage of the spatially hyperbolic character of the equations (ref. 13).

obtained here from the same time accurate method (time approaching infinity) used to obtain the perturbation solution.[2]

This study is restricted to the two-dimensional flow of an inviscid perfect gas. The Eulerian gasdynamic equations in conservation form were chosen rather than the potential equation. The choice of the form of the equations of motion was somewhat arbitrary and a similar study with the potential equation seems warranted. The potential equation solution requires less computer storage and is generally the form best suited to relaxation methods. On the other hand, vorticity in the flow field (resulting from the unsteady motion of lifting bodies) and the embedded shock motion are probably most easily computed with the conservation form of the Eulerian equations. The most efficient choice (potential or Eulerian) remains to be determined.

More approximate methods of solution (e.g., the mixing of supersonic and subsonic linear theory (refs. 14 and 15)) should not be excluded from consideration for transonic problems. The computation time required for such solutions could be considerably less than the present approach; however, considerable finesse is required in choosing the proper mixing. The solutions obtained by the finite-difference methods should be useful in developing more efficient approximate methods.

The numerical, explicit, third-order-accurate, finite-difference scheme and the equations of motion are given in section I. Previously unpublished details of the difference scheme are presented in the Appendix. Solutions for subsonic nonlifting and lifting airfoils are presented in section II and section III, respectively. Sections II and III indicate the adequacy of the numerical method in comparison with exact, linear, time-dependent solutions. Section IV reviews the use of indicial functions and their relation to the oscillatory aerodynamic coefficients. Numerically determined (via indicial function) oscillatory coefficients are compared with subsonic linear theory coefficients. Section V presents the results of a numerical analysis of a biconvex circular arc airfoil oscillating about midchord at transonic speeds. Comparisons are made between oscillatory moment coefficients obtained from linear theory, numerical solution, and wind-tunnel experiments.

I. NUMERICAL METHOD

The gasdynamic equations for two-dimensional, unsteady, inviscid flow are expressed in conservative (or divergence law) form as

$$\frac{\partial U}{\partial t} + \frac{\partial F}{\partial x} + \frac{\partial G}{\partial y} = 0 \tag{2}$$

where t, x, and y represent the time and Cartesian space coordinates and U, F, and G are the vectors:

[2]In this study, the variable coefficient partial differential equations are not explicitly programmed. Rather the perturbation is made from the converged (nonuniform steady state) solution to the nonlinear equations.

$$U = \begin{bmatrix} \rho \\ \rho u \\ \rho v \\ e \end{bmatrix}, \quad F = \begin{bmatrix} \rho u \\ \rho u^2 + p \\ \rho uv \\ (e + p)u \end{bmatrix}, \quad G = \begin{bmatrix} \rho v \\ \rho uv \\ \rho v^2 + p \\ (e + p)v \end{bmatrix} \tag{3}$$

The variables in equations (3) are the density ρ, the velocity components u and v, pressure p, and total energy per unit volume e. The additional required equation is the equation of state (for a perfect gas):

$$p = (\gamma - 1)\left[e - \frac{\rho}{2}(u^2 + v^2)\right] \tag{4}$$

where γ, a constant, is equal to the ratio of specific heats (taken as 1.4 here). The conservative form of the Eulerian equations was chosen for its "shock-capturing" capabilities (ref. 16).

The numerical method is an explicit, third-order, noncentered, finite-difference scheme introduced by Warming, Kutler, and Lomax (ref. 17). The method is uniformally third-order-accurate in both time and spatial increments. The basic scheme applied to equation (2) takes the form:

$$U^{(1)}_{j,k} = U^n_{j,k} - \frac{2}{3}\left\{\frac{\Delta t}{\Delta x}\left[F^n_{j+1,k} - F^n_{j,k}\right] + \frac{\Delta t}{\Delta y}\left[G^n_{j,k+1} - G^n_{j,k}\right]\right\} \tag{5a}$$

$$U^{(2)}_{j,k} = \frac{1}{2}\left(U^n_{j,k} + U^{(1)}_{j,k}\right) - \frac{1}{3}\left\{\frac{\Delta t}{\Delta x}\left[F^{(1)}_{j,k} - F^{(1)}_{j-1,k}\right] + \frac{\Delta t}{\Delta y}\left[G^{(1)}_{j,k} - G^{(1)}_{j,k-1}\right]\right\} \tag{5b}$$

$$\begin{aligned} U^{n+1}_{j,k} = U^n_{j,k} - \frac{1}{24}\Bigg\{ & \frac{\Delta t}{\Delta x}\left(-2F^n_{j+2,k} + 7F^n_{j+1,k} - 7F^n_{j-1,k} + 2F^n_{j-2,k}\right) \\ & + \frac{\Delta t}{\Delta y}\left(-2G^n_{j,k+2} + 7G^n_{j,k+1} - 7G^n_{j,k-1} + 2G^n_{j,k-2}\right) \\ & + w_x\left(U^n_{j+2,k} - 4U^n_{j+1,k} + 6U^n_{j,k} - 4U^n_{j-1,k} + U^n_{j-2,k}\right) \\ & + w_y\left(U^n_{j,k+2} - 4U^n_{j,k+1} + 6U^n_{j,k} - 4U^n_{j,k-1} + U^n_{j,k-2}\right)\Bigg\} \\ & - \frac{3}{8}\left\{\frac{\Delta t}{\Delta x}\left(F^{(2)}_{j+1,k} - F^{(2)}_{j-1,k}\right) + \frac{\Delta t}{\Delta y}\left(G^{(2)}_{j,k+1} - G^{(2)}_{j,k-1}\right)\right\} \end{aligned} \tag{5c}$$

where

$$U^{(1)}_{j,k} = U^{(1)}(j\Delta x, k\Delta y), \text{ etc.} \tag{5d}$$

and ω_x and ω_y are free parameters that may be selected to minimize dispersion or dissipation but must be properly selected to obtain a stable numerical solution (see the Appendix and ref. 17.)

During the development of the computer program, the shock resolution was not satisfactory when the basic scheme (eqs. (5)) was used throughout the flow. In particular, a nonphysical oscillation near the shock produced a distorted pressure distribution upstream of the shock. Similar problems were encountered by investigators who used relaxation techniques (refs. 10 and 11). They found that the use of upwind difference schemes in the supersonic region resolved the difficulties. Accordingly, the program was modified to use the skewed upwind differencing scheme (described in the Appendix) for the supersonic portion of the flow. The method retains third-order accuracy in time and space. If j represents the streamwise (j increases downstream) direction, the skewed differencing scheme is based on points j-3, j-2, j-1, j, and j+1. The specific differencing formulas are unchanged for the first and second steps; however, the final step (corresponding to eq. (5c)) becomes

$$
\begin{aligned}
U^{n+1}_{j,k} = U^{n}_{j,k} - \frac{1}{24}\Bigg\{ & \frac{\Delta t}{\Delta x}\left(-2F^{n}_{j-3,k} + 3F^{n}_{j-2,k} - 7F^{n}_{j,k} + 6F^{n}_{j+1,k}\right) \\
& + \frac{\Delta t}{\Delta y}\left(-2G^{n}_{j,k+2} + 7G^{n}_{j,k+1} - 7G^{n}_{j,k-1} + 2G^{n}_{j,k-2}\right) \\
& + \omega_{xs}\left(U^{n}_{j-3,k} - 4U^{n}_{j-2,k} + 6U^{n}_{j-1,k} - 4U^{n}_{j,k} + U_{j+1,k}\right), \\
& + \omega_{y}\left(U^{n}_{j,k+2} - 4U^{n}_{j,k+1} + 6U^{n}_{j,k} - 4U^{n}_{j,k-1} + U^{n}_{j,k-2}\right)\Bigg\} \\
& - \frac{3}{8}\left\{\frac{\Delta t}{\Delta x}\left(3F^{(2)}_{j,k} - 4F^{(2)}_{j-1,k} + F^{(2)}_{j-2,k}\right) + \frac{\Delta t}{\Delta y}\left(G^{(2)}_{j,k+1} - G^{(2)}_{j,k-1}\right)\right\} \qquad (6)
\end{aligned}
$$

where ω_{xs} is a free parameter similar to ω_x and ω_y.

For the present study, the flow tangency boundary condition is applied on the coordinate line instead of on the airfoil surface. This approximation is adequate for many steady transonic airfoil calculations. The boundary conditions for the far field were set equal to free stream. The effects of the outer boundaries were diminished and the resolution of the near-field was increased by coordinate stretching.

All computations were made on an IBM 360-67, coupled with an interactive graphics system. The graphics display was invaluable in checking out the program and in selecting the free parameters ω_x, ω_y, and ω_{xs} and the optimal time step Δt.

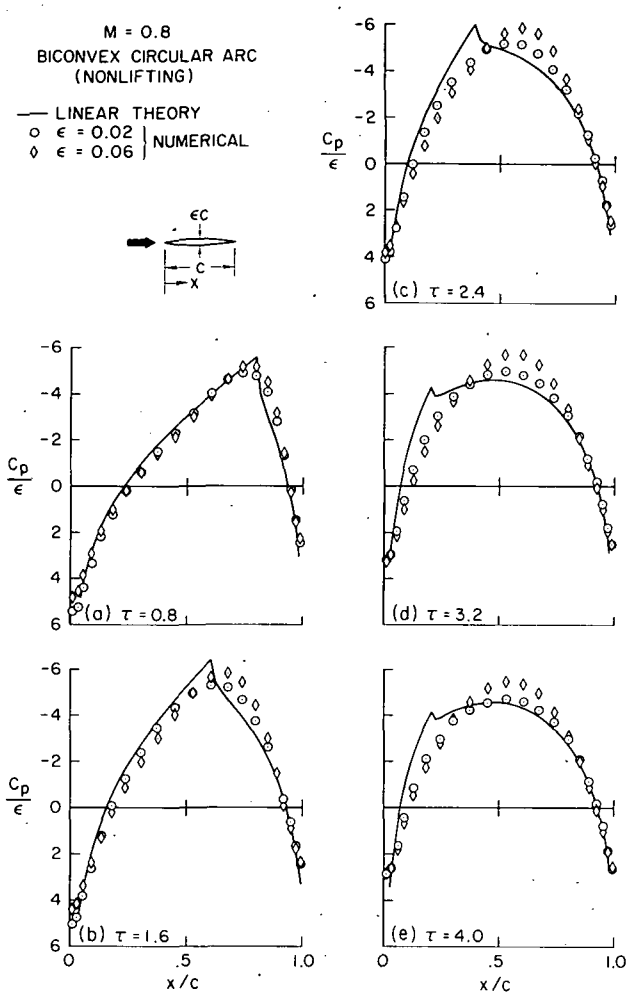

Figure 1.— Chordwise pressure coefficient, c_p, at various times, τ, following an indicial velocity change, U_∞, at $\tau = 0$.

To test the adequacy of the numerical solution for subcritical noncirculatory flows, the transient solution for a nonlifting biconvex circular arc airfoil was computed. The transient pressure coefficient distributions are presented in figure 1. The initial conditions were uniform free stream ($M_\infty = 0.8$). The physical analogy is an airfoil accelerated from rest instantaneously to the free-stream velocity (step change in streamwise velocity component). Numerical results are shown for two thickness-to-chord ratios ($\varepsilon = 0.02$ and 0.06) at several time increments, $\tau = U_\infty t/c$, where τ is the number of chords traveled. The linear theory solutions were obtained by Lomax using methods similar to those in reference 3 and are presented for comparison.

Several observations are useful in interpreting the results shown in figure 1. The discontinuities of the pressure gradient (c_p slope) predicted by linear theory do not appear in the numerical solutions for two reasons, one numerical and one physical. The numerical method tends to smooth these discontinuities because of the limited resolution (note that the linear theory pulse length is approximately the order of the numerical grid spacing) and numerical dissipation and dispersion. The physics introduces nonlinear terms in the equation of motion which are included in the numerical solution but are neglected by the linear theory. These nonlinearities can become important in regions of large pressure gradient changes, thus limiting the applicability of the linear theory.

Note the significant difference in the two numerical solutions for different thickness ratios. Note especially the lag of the receding wave in figures 1(b), (c), and (d) and the greater pressure changes for the thicker airfoil. These effects should be anticipated because of the higher local Mach numbers and lower upstream propagation rates for thicker airfoils. The critical pressure coefficient c_p^* (for $M = 0.8$) is 0.4346; thus the local Mach numbers approach unity for the thicker airfoil ($c_p^*/\varepsilon = 7.24$ for $\varepsilon = 0.06$).

III. FLOWS WITH CIRCULATION (LIFTING AIRFOILS)

One of the test cases for circulatory flow was a flat plate with lateral velocity (sinking or plunging). The initial conditions correspond to a step change in the lateral (normal to free stream) velocity component. The computed differential pressure distributions for several time steps are shown in figure 2. The amplitude of the lateral velocity component for the numerical solution was chosen to correspond to an equivalent angle of attack (v/U_∞) of 1°. For this small perturbation, the agreement with linear theory should be good except for (1) the discontinuities in the pressure gradient predicted by the linear theory (as discussed in the previous section) and (2) the pressure coefficients near the leading edge where the linear theory predicts a weak singularity with infinite velocities.

One advantage of using the full Eulerian equations (as opposed to the potential equation) is the ability to compute circulatory flow. For example, the transient motion of the sinking airfoil produces a vortex distribution in the wake that is swept downstream by the flow. Figure 3 compares the numerically computed wake circulation and that predicted by linear theory (ref. 3). The numerical values were obtained by evaluating a line integral around the wake at each time step of the numerical integration of the equations of motion.

The section lift coefficient is obtained by integrating the chordwise pressure distribution. If the pressure distributions are those resulting from a step change in velocity of the airfoil, then the resulting lift coefficient time history $c_{\ell_\alpha}(\tau)$ is called the indicial lift coefficient. The

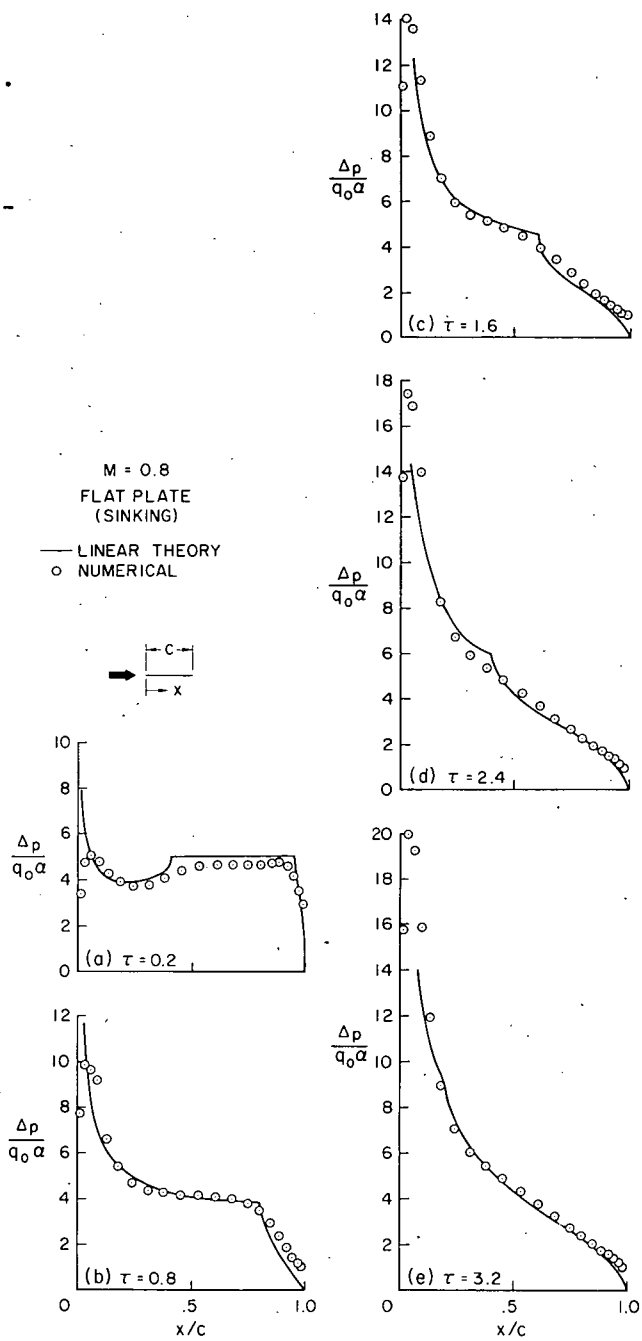

Figure 2.— Chordwise lifting pressure, Δp, at various times, τ, following indicial sinking velocity, v_o, at $\tau = 0$.

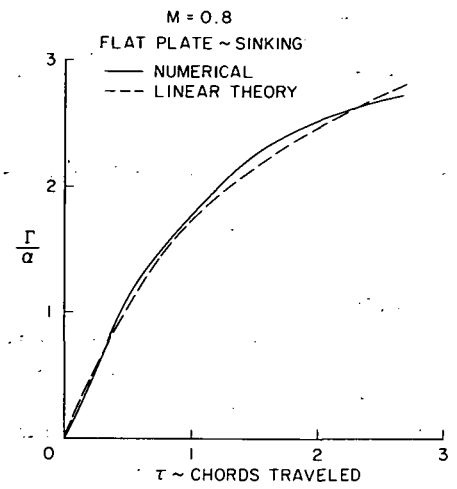

Figure 3.— Circulation, Γ, following an indicial sinking velocity, v_o, at $\tau = 0$.

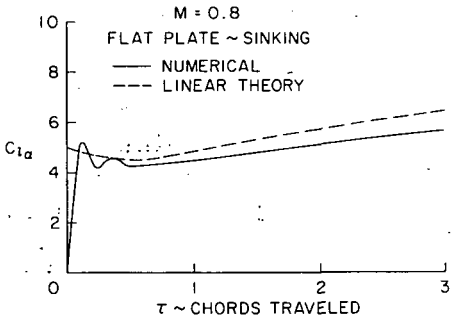

Figure 4.— Indicial lift coefficient, c_{ℓ_α}, for an indicial sinking velocity, v_o, at $\tau = 0$.

numerically determined indicial lift coefficient for the sinking flat plate is shown in figure 4. The integrals of the numerically computed pressure distributions (fig. 2) were obtained by use of the trapezoidal rule, while the linear theory integrals were obtained analytically and include the linear theory, leading-edge singularity.

A discussion of the numerical oscillations near $\tau = 0$ (fig. 4) is important since they indicate the maximum resolvable frequency of the numerical method. The frequency is proportional to the inverse of the grid spacing and the inverse of the Mach number. In terms of reduced frequency, k, the maximum resolvable frequency is of order $1/M_\infty\Delta$, that is,

$$k_{max} = 0\left(\frac{1}{M_\infty\Delta}\right) \tag{7}$$

where Δ is the grid spacing made dimensionless with respect to the chord and M_∞ is the free-stream Mach number. This does not present a severe limitation since a grid spacing of 1/20 the chord at $M = 1$ produces $k_{max} = 0(20)$, which is sufficiently above the range of most dynamic and aeroelastic investigations. The oscillations shown in figure 4 correspond to a reduced frequency of approximately 15.

IV. INDICIAL FUNCTIONS AND OSCILLATORY AERODYNAMIC COEFFICIENTS

Although one can integrate the nonlinear equations of motion (eq. (2)) for given initial conditions and time-dependent boundary conditions as in section II, the results have very restricted use since superposition of solutions (the basis of most flutter analysis) is no longer applicable. If oscillatory solutions to the nonlinear equations are desired, the computation must be done for each frequency and each amplitude of oscillation and the coefficients are valid only for the motion (or modal function) assumed for the calculation (i.e., superposition of modal functions to obtain other motions is not applicable).

The most productive area for the numerical investigation of unsteady transonic phenomena appears to be the small-perturbation unsteady motion about the nonuniform flow conditions (as outlined in the Introduction) (linear perturbation about nonlinear steady state). This type of linearization produces aerodynamic coefficients applicable to a particular airfoil geometry (as opposed to linear thin airfoil theory that has the same unsteady coefficients for all thickness and camber distributions) and the superposition of modal functions allows the application of conventional flutter methods.

In the classical linear analysis of unsteady motion of airfoils, two different but compatible approaches are taken. In one method, it is assumed initially that the solution depends harmonically on time (refs. 1, 2, 4, and 5). For flutter analysis, the solutions (lift and moment coefficients) are tabulated as a function of reduced frequency and Mach number and are used in the airfoil equations of motion with the assumption that the motion is harmonic in time at the flutter (stability) boundary (ref. 18). If the solution is known for each frequency, the solution for the general time history is obtained with the aid of Fourier transforms (ref. 19). Although this method can be used to obtain general time histories, it is seldom used in practice since the oscillatory solutions are generally of primary importance.

The second but less often used method for the linear analysis of unsteady motions is the indicial function approach (refs. 3 and 20). For example, if an airfoil is given an instantaneous sinking velocity (i.e., a discontinuous step change in velocity), the resulting flow field is the indicial response. For a given step change in motion (sinking, pitching, etc.), the solutions (generally in terms of lift and moment coefficients) can be tabulated as a function of time and, with the aid of Duhamel's integral, they can be used to compute the solution for a general time history of airfoil motion. The oscillatory aerodynamic coefficients can be obtained by Fourier transforms of the indicial coefficients (refs. 3 and 20).

Each approach can be used to obtain oscillatory aerodynamic coefficients by numerical solution of the equations for small perturbation about the steady-state nonuniform flow (linear partial differential equations with variable coefficients). As mentioned in the Introduction, relaxation schemes appear most promising for solving the equations for harmonic motion (time eliminated) and time accurate methods appear best suited for the indicial function approach.

For this study, the indicial function approach and time accurate solution of the Eulerian equations were exploited. The oscillatory aerodynamic coefficients were determined by Fourier transform of the indicial response functions, which requires very little additional computational time. The indicial functions and oscillatory aerodynamic coefficients for sinking and pitching motion are related by:

$$
\left.
\begin{aligned}
L_1(k) &= -\frac{1}{2}\int_0^\infty \Delta c_{\ell_\alpha}(\tau)\cos 2k\tau\, d\tau \\
L_2(k) &= -\left[-\frac{1}{4k}\, c_{\ell_\alpha}(\infty) - \frac{1}{2}\int_0^\infty \Delta c_{\ell_\alpha}(\tau)\sin 2k\tau\, d\tau\right] \\
L_3(k) &= -\frac{1}{4k^2}\left\{c_{\ell_\alpha}(\infty) + 4k^2\int_0^\infty\left[\Delta c_{\ell_q}(\tau)\cos 2k\tau\right.\right. \\
&\qquad \left.\left. - \frac{1}{2k}\,\Delta c_{\ell_\alpha}(\tau)\sin 2k\tau\right] d\tau\right\} \\
L_4(k) &= -\frac{1}{4k^2}\left\{2kc_{\ell_q}(\infty) - 2k\int_0^\infty\left[\Delta c_{\ell_\alpha}(\tau)\cos 2k\tau\right.\right. \\
&\qquad \left.\left. + 2k\Delta c_{\ell_q}(\tau)\sin 2k\tau\right] d\tau\right\} \\
M_1(k) &= -\int_0^\infty \Delta c_{m_\alpha}(\tau)\cos 2k\tau\, d\tau \\
M_2(k) &= -\left[\frac{1}{2k}\, c_{m_\alpha}(\infty) - \int_0^\infty \Delta c_{m_\alpha}(\tau)\sin 2k\tau\, d\tau\right] \\
M_3(k) &= -\frac{1}{2k^2}\left\{c_{m_\alpha}(\infty) + 2k\int_0^\infty\left[-\Delta c_{m_\alpha}(\tau)\sin 2k\tau\, d\tau\right.\right. \\
&\qquad \left.\left. + \Delta c_{m_q}(\tau)2k\cos 2k\tau\right] d\tau\right\} \\
M_4(k) &= -\frac{1}{2k^2}\left\{2kc_{m_q}(\infty) - 2k\int_0^\infty\left[\Delta c_{m_\alpha}(\tau)\cos 2k\tau\, d\tau\right.\right. \\
&\qquad \left.\left. + \Delta c_{m_q}(\tau)2k\sin 2k\tau\right] d\tau\right\}
\end{aligned}
\right\} \qquad (8)
$$

The notation in equations (8) is that of Garrick and Rubinow (ref. 5) for the oscillatory coefficients (L_1, L_2, L_3, L_4, M_1, M_2, M_3, and M_4) and of Lomax, Fuller, and Sluder (ref. 3) for the indicial coefficients (c_{ℓ_α}, c_{m_α}, c_{ℓ_q}, and c_{m_q}). Subscripts α and q refer to sinking and pitching motion, respectively. The function $\Delta c(\tau)$ is defined by $\Delta c(\tau) = c(\infty) - c(\tau)$.

Figure 5 shows the results of a test case for obtaining the oscillatory coefficients using the numerically determined indicial functions. The indicial functions were computed for a sinking flat plate (see section III) and a

flat plate pitching about the leading edge. These were used to compute the indicial function for a plate rotating about the quarter-chord point. This could have been obtained directly by computing the one indicial function for rotation about the quarter-chord point; however, the two indicial functions allow computation of any motion in the plane. Equations (8) were used to obtain M_3 and M_4 plotted in figure 5. Figure 5 also shows the subsonic linear theory results of Timman, van de Vooren, and Greidanus (ref. 2), who solved the boundary value problem for harmonic motion using expansions in terms of Mathieu and modified Mathieu functions. The numerical results compare favorably with the results of Timman *et al.* and adequately predict the low-frequency destabilizing aerodynamic damping (positive M_4, fig. 5(a)).

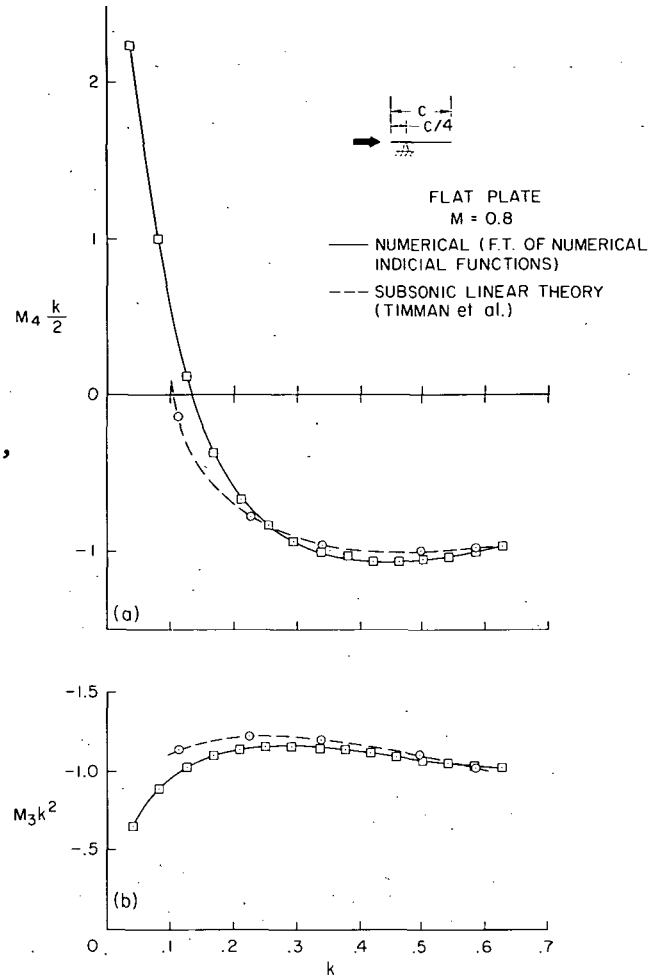

Figure 5.— Oscillatory aerodynamic moment coefficients, M_3 and M_4, for various reduced frequencies k.

The minimum frequency that can be resolved (k_{min}) for a given amount of indicial function computation, τ_{max}, is not well defined and thus requires further investigation. However, the minimum frequency can be no less than $0(\pi/\tau_{max})$

$$k_{min} > 0\left(\frac{\pi}{\tau_{max}}\right) \qquad (9)$$

The approximate range of resolution of reduced frequency can be stated from relations (7) and (9) as

$$0\left(\frac{\pi}{\tau_{max}}\right) < k < 0\left(\frac{1}{M_\infty \Delta}\right) \qquad (10)$$

It was pointed out in section III that the step change in motion can introduce oscillations in the response curve (i.e., fig. 4). The oscillations are not physical but result from the introduction of a finite mesh size by the numerical method. They do not generally present an analysis problem since the frequency k_{max} (eq. (7)) must be kept greater than the maximum frequency of physical interest and the integral terms of equations (8) will effectively filter out the effect of the oscillations. If the amplitude of the oscillations should become sufficiently large, the nonlinear effects in the equations

of motion could produce analysis problems. However, the amplitude of the oscillations can be minimized by the use of a ramp displacement function (finite rise time to steady value) in lieu of a step displacement motion. The rise time of the ramp motion τ_o (i.e., τ_o is the time to reach a constant amplitude of motion) should be chosen equal to the period of the induced oscillations ($2\pi/k_{max}$). The response function for the ramp motion and the response function for the step motion are related (with the aid of Duhamel's integral) by

$$\left.\begin{aligned} c^R(\tau) &= \frac{1}{\tau_o}\int_0^{\tau} c^S(\tau_1)\, d\tau_1 , \quad o \leqslant \tau \leqslant \tau_o \\ c^R(\tau) &= \frac{1}{\tau_o}\int_{\tau-\tau_o}^{\tau} c^S(\tau_1)\, d\tau_1 , \quad \tau_o \leqslant \tau \leqslant \infty \end{aligned}\right\} \tag{11}$$

where superscripts R and S denote ramp and step, respectively. The frequency analysis using the ramp motion is now the same as for a step motion except it is generally more convenient to use the mean value approximation to evaluate the integrals in equations (8) rather than to differentiate $c^R(\tau)$ to obtain $c^S(\tau)$.

V. ANALYSIS OF CIRCULAR ARC AIRFOIL OSCILLATING IN TRANSONIC FLOW

Subsonic linear theory predicts that an airfoil oscillating at low reduced frequency about a point at or forward of the quarter-chord point will have negative or destabilizing aerodynamic damping (ref. 4) (e.g., section IV and fig. 5(a)). For rotation about points aft of the quarter-chord, subsonic linear theory predicts stabilizing aerodynamic damping for all reduced frequencies. However, experimental wind-tunnel tests by Bratt and Chinneck (ref. 21) of a 7-1/2-percent thick biconvex airfoil oscillating about midchord exhibit an aerodynamic instability for a narrow range of subsonic free-stream Mach number (positive $m_{\dot\theta}$, fig. 6(a)). The aerodynamic stiffness moment, m_θ, also decreases (fig. 6(b)), contrary to the prediction of linear subsonic theory. Experimental investigators believed that these effects were related to shock waves that formed on the surface of the airfoil; therefore, this model was chosen for numerical investigation.

The procedure for obtaining numerical data points involved three steps at each Mach number investigated. First, the steady-state nonlifting solution was computed, then the indicial functions were computed, and finally the oscillatory moment coefficients were computed using equations (8). Results of the numerical investigation are shown in figure 7.

The experimental data of Bratt and Chinneck were obtained at very low reduced frequencies (k = 0.004) — below the general range of flutter investigation and below the minimum reduced frequency (k = 0.040) of the present numerical calculations (eq. (10)). To present a quantitative correlation

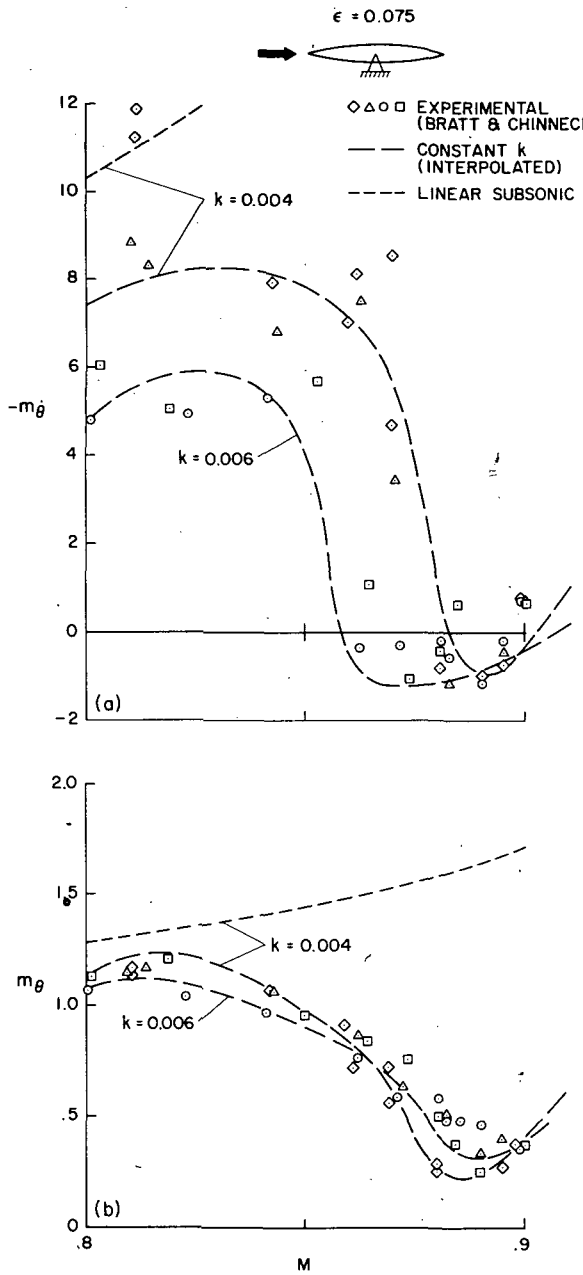

Figure 6.— Experimental oscillatory aerodynamic moment coefficients for biconvex circular arc airfoil rotating abount midchord.

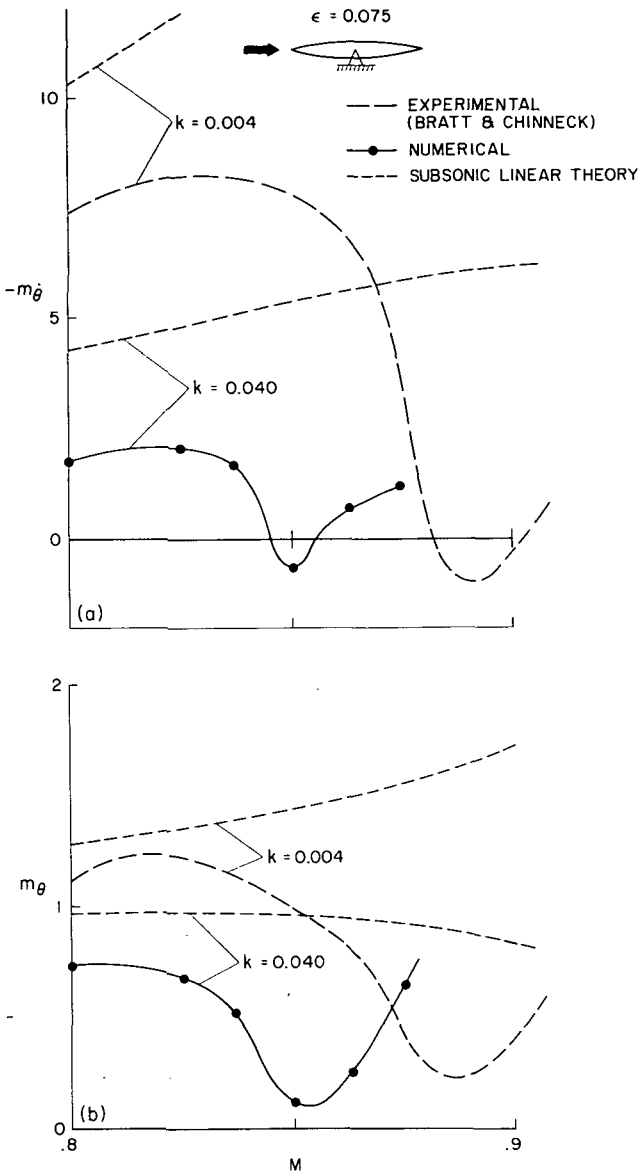

Figure 7.— Oscillatory aerodynamic damping ($m_{\dot{\theta}}$) and stiffness (m_θ) moment coefficients for biconvex circular arc airfoil oscillating about midchord.

between the numerical and experimental data obtained for different reduced frequencies, the subsonic linear theory results for the corresponding reduced frequencies are also shown in figure 7. The numerical results predict the negative damping and the decrease in stiffness moment obtained in the experiments.

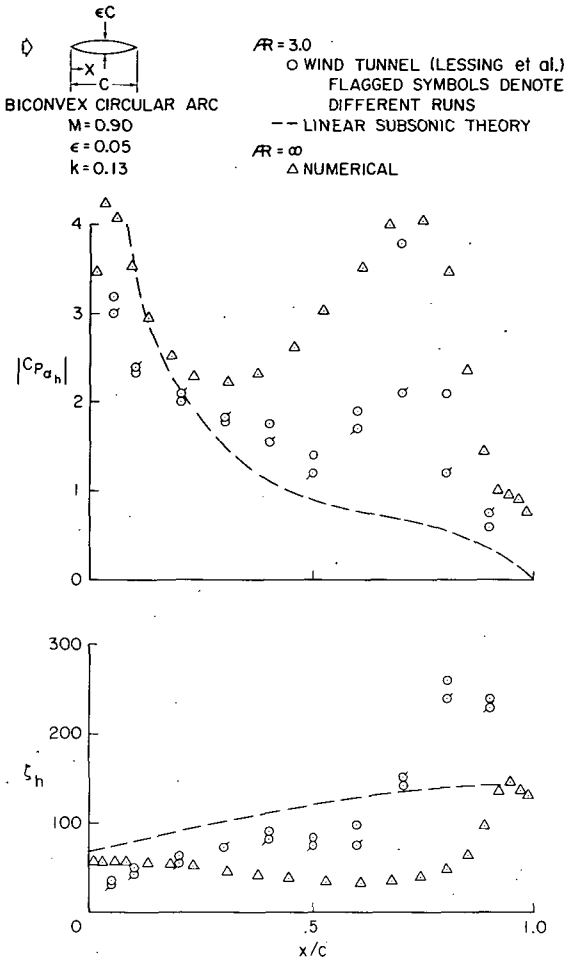

Figure 8.— Chordwise oscillatory pressure coefficient and phase angle for biconvex circular arc airfoil oscillating normal to free stream (plunging).

Chordwise pressure distributions were not measured by Bratt and Chinneck in the experiments discussed previously. Experimental pressure distributions were obtained by Lessing, Troutman, and Menees (ref. 22) for a 5-percent-thick biconvex airfoil oscillating in bending (each spanwise section sinking). Although the experimental model had a low aspect ratio ($AR = 3.0$) and there were three-dimensional effects, the chordwise pressure distribution at the quarter span station (midway between the fixed end and the tip) provides a qualitative comparison for experimental and numerical results (fig. 8). The results are presented for the same reduced frequency and free-stream Mach number. The greatest disparity between the three-dimensional experimental data and the two-dimensional numerical results is, as anticipated, in the phase angle ζ_h. While the qualitative agreement of pressure coefficient, $c_{p_{\alpha_h}}$, seems satisfactory, quantitative correlation must await three-dimensional numerical results.

CONCLUSIONS AND RECOMMENDATIONS FOR FUTURE INVESTIGATION

Pressure distributions obtained by numerically integrating the two-dimensional unsteady Eulerian equations were presented. The applicability and efficiency of the numerical indicial function method were outlined. Subsonic and transonic oscillatory aerodynamic coefficients were computed and compared with those obtained from subsonic linear theory and transonic wind-tunnel data. The results of this study substantiate the feasibility of obtaining unsteady transonic aerodynamic data by numerically integrating the gas-dynamic equations of motion.

The following topics are recommended for future investigations.

(1) Since aerodynamic strip theory is not generally applicable in the transonic flow range, the present study should be extended to include three-dimensional flows.

(2) The numerical integration of the unsteady potential equation should be investigated in a study similar to the present one. The lower computer storage requirement should be advantageous.

(3) The optimum numerical method for obtaining oscillatory aerodynamic coefficients has not been resolved. Therefore, the application of relaxation methods should be investigated. The methods may prove particularly efficient for low reduced frequencies and for cases where coefficients are required at only a few reduced frequencies.

(4) The more approximate methods for unsteady transonic flow analysis (e.g., those that mix the results of linear subsonic and supersonic theory) should also be pursued since they could require significantly less computer time. The results of the direct integration methods of the type used here should be useful in developing more approximate methods.

Ames Research Center
National Aeronautics and Space Administration
Moffett Field, Calif. 94035, November 27, 1973

APPENDIX

UPWIND THIRD-ORDER SCHEME

This appendix describes an "upwind" third-order difference scheme that was used in the supersonic region of the transonic calculations described in this report. To review briefly, the basic noncentered third-order scheme was developed in reference 17. For a one-dimensional hyperbolic system in the conservation law form

$$\frac{\partial U}{\partial t} + \frac{\partial F(U)}{\partial x} = 0 \ , \tag{A1}$$

the scheme is

$$U_j^{(1)} = U_j^n - \frac{2\Delta t}{3} \frac{\Delta F_j^n}{\Delta x} \tag{A2a}$$

$$U_j^{(2)} = \frac{1}{2}\left(U_j^n + U_j^{(1)}\right) - \frac{\Delta t}{3} \frac{\nabla F_j^{(1)}}{\Delta x} \tag{A2b}$$

$$U_j^{n+1} = U_j^n - \frac{\Delta t}{4}\left(1 - \frac{2}{3}\delta^2\right) \frac{\mu\delta}{\Delta x} F_j^n - \frac{3}{4}\Delta t \frac{\mu\delta}{\Delta x} F_j^{(2)} - \frac{\omega}{24}\delta^4 U_j^n \tag{A2c}$$

where the conventional difference operators are defined by

$$\Delta U_j^n = U_{j+1}^n - U_j^n \ , \quad \nabla U_j^n = U_j^n - U_{j-1}^n$$

and

$$\mu\delta U_j^n = \left(U_{j+1}^n - U_{j-1}^n\right)/2 \ , \quad \delta^2 U_j^n = U_{j+1}^n - 2U_j^n + U_{j-1}^n$$

and

$$F_j^{(1)} = F^{(1)}\left(U_j^{(1)}\right), \quad F_j^{(2)} = F^{(2)}\left(U_j^{(2)}\right)$$

The predictor $U_j^{(1)}$ and the first corrector $U_j^{(2)}$ are evaluated at time $(n+2/3)\Delta t$ and together constitute MacCormack's second order algorithm (ref. 17). The algorithm (A2) is called a noncentered scheme because it uses noncentered difference quotients to approximate $\partial F/\partial x$ in the first two steps.

The fourth-order spatial operator δ^4 of equation (A2c) with the multiplicative parameter ω is necessary to achieve numerical stability.

The von Neumann stability analysis of the scheme (A2) as described in reference 17 was based on the application of the scheme to the following linearized version of the hyperbolic system (A1):

$$\frac{\partial U}{\partial t} + A \frac{\partial U}{\partial x} = 0 \tag{A3}$$

where A is the Jacobian matrix $\partial F/\partial U$ (A is assumed constant). A necessary and sufficient condition for stability is

$$4\nu^2 - \nu^4 \leq \omega \leq 3 , \quad |\nu| = |\sigma|\Delta t/\Delta x \leq 1$$

for all eigenvalues σ of A. The range of ω for a stable algorithm is shown by the shaded region in figure 9. The dashed curve of the figure is the value of ω that minimizes dispersive error (ref. 17).

The scheme (A2) uses numerical data from the five spatial points x_j, $x_{j\pm1}$, and $x_{j\pm2}$ at time level n to advance the solution one time step. A third-order upwind scheme can be devised that uses data at four points, say x_j, $x_{j\pm1}$, and x_{j-2}, to advance the solution. However, to avoid undue complication in programming logic, the condition was imposed that the formulas for $U_j^{(1)}$ and $U_j^{(2)}$ (as given by eqs. (A2a) and (A2b)) be the same throughout the computational region. This led to the construction of the following upwind algorithm that uses data from the five points x_j, $x_{j\pm1}$, x_{j-2}, and x_{j-3} to advance the solution:

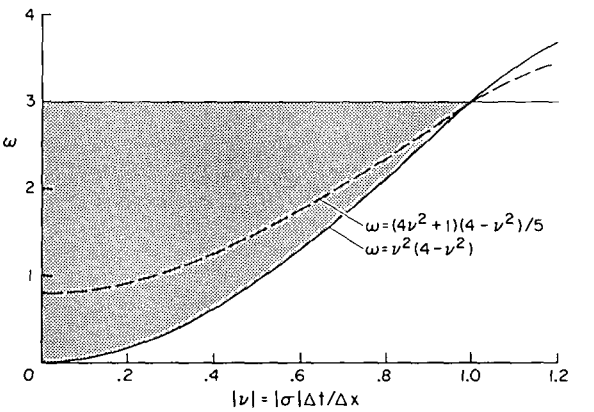

Figure 9.— Stable range of free parameter ω and ν for basic third-order scheme.

$$U_j^{(1)} = \text{same as right side of equation (A2a)} \tag{A4a}$$

$$U_j^{(2)} = \text{same as right side of equation (A2b)} \tag{A4b}$$

$$U_j^{n+1} = U_j^n - \frac{\Delta t}{4}\left(1 + \Delta - \frac{1}{2}\nabla + \frac{1}{3}\nabla^2\right)\frac{\nabla F_j^n}{\Delta x} - \frac{3}{4}\Delta t\left(1 + \frac{1}{2}\nabla\right)\frac{\nabla F_j^{(2)}}{\Delta x} - \frac{\omega}{24}E\nabla^4 U_j^n \tag{A4c}$$

where E is the shift operator $EU_j^n = U_{j+1}^n$. The last difference operator on the right of equation (A4c) is a fourth-order operator that is analogous to the free parameter term on the right in equation (A2c).

The remainder of this appendix outlines a linear stability analysis of the upwind scheme (A4). The procedure is essentially the same as for the basic third-order scheme (A2) (see ref. 17 for a more detailed discussion). To perform the von Neumann (Fourier) stability analysis, the algorithm (A4) is applied to a linearized equation (A3). A further simplification accrues if one applies the algorithm to the linear scalar equation

$$\frac{\partial u}{\partial t} + c\,\frac{\partial u}{\partial x} = 0 \tag{A5}$$

rather than equation (A3). Whatever stability bound results by application of the algorithm to equation (A5) is valid for the linear system (A3) if c is replaced by σ (the eigenvalues of A). When applied to the linear equation (A5), the algorithm (A4) can be reduced to a single-step difference operator if one inserts equation (A4a) into (A4b) and the result into (A4c); thus,

$$u_j^{n+1} = u_j^n - \frac{1}{4}\nu(4 + \Delta + \nabla + \frac{1}{3}\nabla^2)\nabla u_j^n + \frac{1}{2}\nu^2(1 + \frac{1}{2}\nabla)\nabla\mu\delta u_j^n$$

$$- \frac{1}{6}\nu^3(1 + \frac{1}{2}\nabla)\nabla\delta^2 u_j^n - \frac{\omega}{24}E\nabla^4 u_j^n \tag{A6}$$

where $\nu = c\,\Delta t/\Delta x$. To determine the amplification factor $g(k)$, each term u_j^n in equation (A6) is replaced by the k-th Fourier component $v^n(k)\exp(ikj\Delta x)$ where $v^n(k)$ denotes the k-th Fourier coefficient. The coefficients at $n+1$ and n are related by

$$v^{n+1}(k) = g(k)v^n(k)$$

The stability of the linear difference equation is ensured if $|g(k)| \le 1$ for all values of k. The square of the modulus of the amplification factor for equation (A6) can be expressed as

$$|g(k)|^2 = 1 - \frac{4}{9}z^2S(z)$$

where

$$z = \sin^2(\theta/2)\,, \qquad \theta = k\Delta x$$

and $S(z)$ is the following quadratic in z:

$$S(z) = 3[\omega + \nu^2(\nu^2 + 2)] - 2(1 - \nu)^2[3\omega + \nu(2\nu^3 + 4\nu^2 + 5\nu - 6)]z$$

$$+ [-\omega^2 - 2\nu\omega(4\nu^2 - 3\nu + 2) + 3\nu^2(1 - 2\nu)(2\nu^3 + \nu^2 - 4\nu + 4)]z^2$$

A necessary and sufficient condition for stability is that

$$S(z) \geq 0 \quad \text{for} \quad 0 \leq z \leq 1$$

The stability constraint on the free parameter ω is found by evaluating $S(z)$ in the small and large wave number limit, i.e., $k = 0$ and $k = \pi/\Delta x$:

$$S(0) = 3[\omega + \nu^2(\nu^2 + 2)] \geq 0$$

$$S(1) = [-\omega + 4\nu(1 - \nu^2)][\omega + 4\nu^3 - 4\nu + 3] \geq 0$$

Hence, there follows

$$-\nu^2(\nu^2 + 2) \leq \omega \leq 4\nu(1 - \nu^2)$$

The two boundary curves for ω are plotted in figure 10 as a function of ν. Clearly, equation (A6) is a stable algorithm for $0 \leq \nu \leq 1$ with $\omega = 0$. This is not the case for the basic third-order scheme (A2), where a non-zero value of ω is essential for stability (see fig. 9).

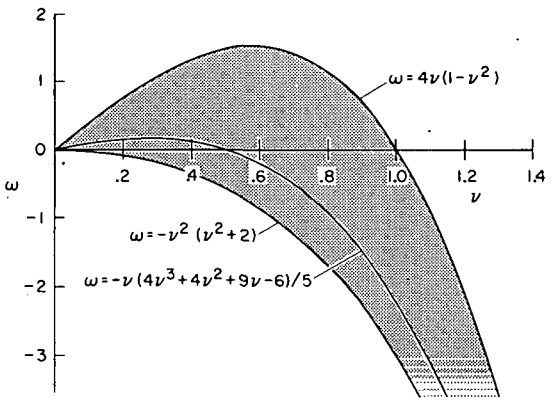

Figure 10.— Stable range of the free parameter ω and $\nu = 1$ upwind third-order scheme.

If the free parameter term in the last step of equation (A4) is retained, then a practical criterion for choosing the parameter ω can be deduced from the modified equation (ref. 17). The modified equation represents the actual differential equation solved when a numerical solution is computed using a finite-difference equation. For the upwind algorithm (A6), the modified equation is

$$\frac{\partial u}{\partial t} + c\,\frac{\partial u}{\partial x} = \sum_{p=4}^{\infty} \mu(p)\,\frac{\partial^p u}{\partial x^p} \tag{A7}$$

where the first two coefficients are

$$\mu(4) = -\frac{\Delta x^4}{24\Delta t}\left[\omega + \nu^2(\nu^2 + 2)\right]$$

$$\mu(5) = \frac{\Delta x^5}{24\Delta t}(1 - \nu)\left[\omega + \frac{\nu(4\nu^3 + 4\nu^2 + 9\nu - 6)}{5}\right]$$

The even-order spatial derivatives on the right side of equation (A7) correspond to dissipative effects and the odd-order spatial derivatives correspond to dispersive effects. The dispersive error of algorithm (A6) can be minimized by choosing ω so that $\mu(5)$ is zero. In this case,

$$\omega = -\nu(4\nu^3 + 4\nu^2 + 9\nu - 6)/5$$

A curve corresponding to this formula is plotted in figure 10. Past experience (refs. 13 and 17) indicates that oscillations in the neighborhood of a discontinuity (shock) can be reduced if ω is chosen for minimum dispersion.

One of the primary advantages of noncentered finite-difference schemes (refs. 13 and 17) is that a scheme constructed for one spatial dimension can be directly generalized to two or more spatial dimensions. Computation of the supersonic region of the two-dimensional transonic flow described in this paper used the basic third-order scheme (A2) in the y-direction and the upwind third-order scheme (A4) in the x-direction. The algorithm is given in detail by equations (5a), (5b), and (6) of the text.

For the applications in this report, the ω corresponding to minimum dispersion was selected for the basic scheme (fig. 9). The same criteria could not be used for the upwind scheme because of the nature of the stability boundaries (fig. 10). The minimum dispersion value of ω that corresponds to the maximum value of $|\nu|$ is no longer a sufficient condition for stability and care must be taken to ensure stability for the minimum value of $|\nu|$ as well. For example, the one-dimensional Eulerian equations have the eigenvalues u, $u + c$, and $u - c$. For supersonic flow, let $u = c + \lambda c$ ($\lambda \geqslant 0$); the eigenvalues then become $(2 + \lambda)c$, $(1 + \lambda)c$, and λc. If the upwind scheme is applied throughout the supersonic zone (i.e., $u \geq c$), then $\lambda = 0$, $\sigma_{min} = 0$, $|\nu|_{min} = 0$, and ω must be set equal to zero for numerical stability (fig. 10). However, if the upwind scheme is applied only in regions where the local velocity exceeds the local speed of sound by a fixed amount (i.e., $\lambda \neq 0$), then $|\nu|_{min} \neq 0$ and nonzero values of ω may be selected to more closely approximate the value of ω for minimum dispersion.

REFERENCES

1. Timman, R.; van de Vooren, A. I.; and Greidanus, J. H.: Aerodynamic Coefficients of an Oscillating Airfoil in Two-Dimensional Subsonic Flow. J. Aeronaut. Sci., vol. 21, no. 7, July 1954, pp. 499-500.

2. Timman, R.; van de Vooren, A. I.; and Greidanus, J. H.: Aerodynamic Coefficients of an Oscillating Airfoil in Two-Dimensional Subsonic Flow. J. Aeronaut. Sci., vol. 18, no. 12, Dec. 1951, pp. 792-802.

3. Lomax, Harvard; Heaslet, Max A.; Fuller, Franklyn B.; and Sluder, Loma: Two- and Three-Dimensional Unsteady Lift Problems in High-Speed Flight. NACA Rep. 1077, 1952.

4. Jordan, P. F.: Aerodynamic Flutter Coefficients for Subsonic, Sonic and Supersonic Flow (Linear Two-Dimensional Theory). ARC R.M. 2932, April 1953.

5. Garrick, I. E.; and Rubinow, S. I.: Flutter and Oscillating Air-Force Calculations for an Airfoil in a Two-Dimensional Supersonic Flow. NACA Rep. 846, 1946.

6. Landahl, Marten T.: Unsteady Transonic Flow. Pergamon Press, New York, 1961.

7. Lin, C. C.; Reissner, E.; and Tsien, H. S.: On Two-Dimensional Non-Steady Motion of a Slender Body in a Compressible Fluid. J. Math. Phys., vol. 27, no. 3, Oct. 1948, pp. 220-231.

8. Miles, J. W.: Linearization of the Equations of Non-Steady Flow in a Compressible Fluid. J. Math. Phys., vol. 33, no. 2, July 1954, pp. 135-143.

9. Magnus, R.; and Yoshihara, H.: Inviscid Transonic Flow Over Airfoils. AIAA J., vol. 8, no. 12, Dec. 1970, pp. 2157-2162.

10. Murman, E. M.; and Cole, J. D.: Calculation of Plane Steady Transonic Flows. AIAA J., vol. 9, no. 1, Jan. 1971, pp. 114-121.

11. Steger, J. L.; and Lomax, H.: Transonic Flow about Two-Dimensional Airfoils by Relaxation Procedures. AIAA J., vol. 10, no. 1, Jan. 1972, pp. 49-54.

12. Bailey, F. R.; and Ballhaus, W. F.: Relaxation Methods for Transonic Flow About Wing-Cylinder Combinations and Lifting Swept Wings. Proceedings of the Third International Conference on Numerical Methods in Fluid Dynamics, no. 19, vol. 2, July 1972, pp. 2-9.

13. Kutler, P.; Warming, R. F.; and Lomax, H.: Computation of Space Shuttle Flow Fields Using Noncentered Finite-Difference Schemes. AIAA J., vol. 11, no. 2, Feb. 1973, pp. 196-204.

14. Cunningham, A. M., Jr.: The Application of General Aerodynamic Lifting Surface Elements to Problems of Unsteady Transonic Flow. NASA CR-112264, 1973.

15. Revell, J. D.: Research on Unsteady Transonic Flow Theory. NASA CR-112114, 1973. Lockheed-California Co.

16. Lax, Peter D.: Weak Solutions of Nonlinear Hyperbolic Equations and Their Numerical Calculation. Comm. Pure Appl. Math., vol. 7, no. 1, Feb. 1954, pp. 159-193.

17. Warming, R. F.; Kutler, P.; and Lomax, H.: Second- and Third-Order Non-centered Difference Schemes for Nonlinear Hyperbolic Equations. AIAA J., vol. 11, no. 2, Feb. 1973, pp. 189-196.

18. Fung, Y. C.: An Introduction to the Theory of Aeroelasticity. John Wiley, 1955.

19. Mazelsky, Bernard: Numerical Determination of Indicial Lift of a Two-dimensional Sinking Airfoil at Subsonic Mach Numbers from Oscillatory Lift Coefficients with Calculations for Mach Number 0.7. NACA TN 2562, 1951.

20. Tobak, Murray: On the Use of the Indicial Function Concept in the Analysis of Unsteady Motions of Wings and Wing-Tail Combinations. NACA Rep. 1188, 1954.

21. Bratt, J. B.; and Chinneck, A.: Measurements of Mid-chord Pitching Moment Derivatives at High Speeds. ARC R.M. 2680, June 1947.

22. Lessing, Henry C.; Troutman, John L.; and Menees, Gene P.: Experimental Determination of the Pressure Distribution on a Rectangular Wing Oscillating in the First Bending Mode for Mach Numbers from 0.24 to 1.30. NASA TN D-344, 1960.

NASA-Langley, 1974 — A-5265

"The aeronautical and space activities of the United States shall be conducted so as to contribute . . . to the expansion of human knowledge of phenomena in the atmosphere and space. The Administration shall provide for the widest practicable and appropriate dissemination of information concerning its activities and the results thereof."

—NATIONAL AERONAUTICS AND SPACE ACT OF 1958

NASA SCIENTIFIC AND TECHNICAL PUBLICATIONS

TECHNICAL REPORTS: Scientific and technical information considered important, complete, and a lasting contribution to existing knowledge.

TECHNICAL NOTES: Information less broad in scope but nevertheless of importance as a contribution to existing knowledge.

TECHNICAL MEMORANDUMS: Information receiving limited distribution because of preliminary data, security classification, or other reasons. Also includes conference proceedings with either limited or unlimited distribution.

CONTRACTOR REPORTS: Scientific and technical information generated under a NASA contract or grant and considered an important contribution to existing knowledge.

TECHNICAL TRANSLATIONS: Information published in a foreign language considered to merit NASA distribution in English.

SPECIAL PUBLICATIONS: Information derived from or of value to NASA activities. Publications include final reports of major projects, monographs, data compilations, handbooks, sourcebooks, and special bibliographies.

TECHNOLOGY UTILIZATION PUBLICATIONS: Information on technology used by NASA that may be of particular interest in commercial and other non-aerospace applications. Publications include Tech Briefs, Technology Utilization Reports and Technology Surveys.

Details on the availability of these publications may be obtained from:

SCIENTIFIC AND TECHNICAL INFORMATION OFFICE

NATIONAL AERONAUTICS AND SPACE ADMINISTRATION

Washington, D.C. 20546